Yanbu Journal of Engineering and Science

Volume 22 | Issue 2 Article 8

2025

Application of Active Fault-Tolerant Control with Hardware Redundancy in Variable Frequency Drives of AC Induction Motors

Zuhair A. Alqarni
Electrical Engineering Department, Al-Baha University ,Al-Aqiq,65779-7738, KSA, zalgarni@bu.edu.sa

Follow this and additional works at: https://yjes.researchcommons.org/yjes
The journal in which this article appears is hosted on Digital Commons, an Elsevier platform.

Recommended Citation
Alqarni, Zuhair A. (2025), Application of Active Fault-Tolerant Control with Hardware Redundancy in Variable Frequency Drives of AC Induction Motors, *Yanbu Journal of Engineering and Science*: Vol. 22: Iss. 2, 88-99.
DOI: https://doi.org/10.53370/1658-5321.1205
Available at: https://yjes.researchcommons.org/yjes/vol22/iss2/8

This Research Article is brought to you for free and open access by Yanbu Journal of Engineering and Science. It has been accepted for inclusion in Yanbu Journal of Engineering and Science by an authorized editor of Yanbu Journal of Engineering and Science.

YANBU JOURNAL OF ENGINEERING AND SCIENCE 2025;22:88–99

Scan the QR to view the full-text article on the journal website

RESEARCH ARTICLE

Application of Active Fault-Tolerant Control with Hardware Redundancy in Variable Frequency Drives of AC Induction Motors

Zuhair A. Alqarni

Electrical Engineering Department, Al-Baha University, Al-Aqiq, 65779-7738, KSA

ABSTRACT

Fault-tolerant control (FTC) techniques have the potential to significantly enhance the dependability of voltage source inverters (VSI) and are becoming popular. This study presents an innovative fault tolerance approach for designing a very dependable induction motor drive (IMD) that incorporates both analytical (active) and hardware redundancies. The created model aims to enhance fault tolerance against the current sensor, speed sensor, and IGBT switch failures in the inverter module. The Active Fault Tolerant Control System (AFTCS) has been applied to the speed sensor to detect any faults in the sensor. If a fault is detected, the system will replace the defective value with an estimated value for open loop speed estimation. This estimation is based on a flux estimation observer. The fault tolerance of the current sensors is designed such that to replace the defective value with the average value of the other two functional current sensors in the event of a failure in one sensor assuming that only one sensor gets faulty at a time. The Fault Detection and Isolation (FDI) unit is designed to rapidly identify and replace a defective switch with a backup redundant switch in the shortest possible timeframe. The stability and convergence of the observer is also proved using the Lyapunov theorem. The use of Markov chains in the reliability investigation further substantiated the system's exceptional dependability. To evaluate the effectiveness of the suggested approach, a variable-speed induction motor with a power capacity of 1.1kW is constructed using MATLAB/Simulink. A 3-phase inverter and fault detector unit are implemented on an STM32-Nucleo-F103RB board with hardware-in-the-loop capability to validate the accuracy of the simulation results to highlight the robustness of the developed active fault-tolerant control. The simulation results coupled with the hardware-in-the-loop experiment demonstrate that the IM drive maintains its stability with little performance degradation in the events of faults in the speed and current sensors as well as inverter switches. Finally, a comparison with the existing literature was carried out to showcase the improved performance and heightened dependability of the proposed model.

Keywords: Fault-tolerant control, Analytical redundancy, Induction motor drive, Open loop observer, Fault-tolerant inverter

1. Introduction

Induction motor (IM) drives are undoubtedly one of the most suitable candidates for different variable speed applications, usually executed in control regimes such as scalar (V/F) control, field-oriented control (FOC), and direct torque control (DTC). Such drive systems are extensively employed in different high-power industrial applications like pumps, machine tool drives, ventilation systems, elevators, process control systems, and electric vehicles (EVs). The reasons for such a widespread deployment of IMs are their robust construction, ample availability in ratings of different ranges, less maintenance requirement, and comparatively low and stable cost over other electrical motors [1].

The extensive utilization of IM demands enhanced reliability of the same in different applications, thereby accelerating the requirement to increase their level of fault tolerance. Fig. 1 shows a diagram, in

Received 23 December 2024; revised 3 February 2025; accepted 10 March 2025.
Available online 2 September 2025

E-mail address: zalgarni@bu.edu.sa (Z. A. Alqarni).

https://doi.org/10.53370/1658-5321.1205
1658-5321/© 2025 The Author(s). Yanbu Journal of Engineering and Science. This is an open access article under the CC BY 4.0 Licence (https://creativecommons.org/licenses/by/4.0/).
Published by Yanbu Industrial College, Saudi Arabia. The journal is hosted on Digital Commons, an Elsevier Platform.

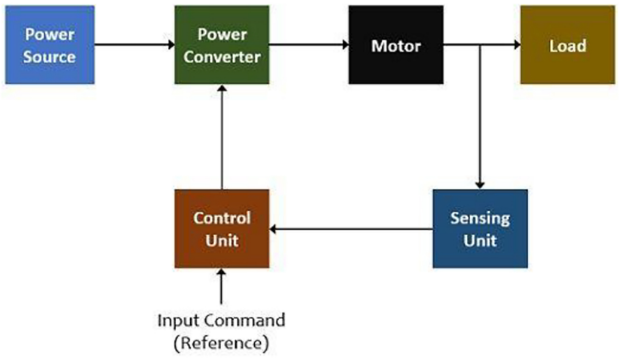

Fig. 1. Block diagram of electric drive system [1].

general, of an electrical drive system. The breakdown of any one of these components may be serious and catastrophic. Hence, online fault monitoring of different components in drive systems is imperative.

Commercially accessible high-performance induction motor (IM) drives have been around since their creation due to their benefits in mechanical durability, decreased size and cost, and field-oriented control or vector control of IM. Feedback signals, such as rotor speed and stator phase currents, often aid the controllers. Consequently, the system's performance will degrade or maybe fail if these sensors experience failure [2].

1.1. Fault-tolerant control

The use of fault-tolerant control (FTC) methods improves machine dependability by mitigating the incidence of faults. When a system stops working altogether, it is declared as failed; when it produces unexpected results, it is declared as having a flaw [3]. An FTC system employs both hardware and analytical redundancy to ensure its reliability. Analytical redundancy may be either passive or aggressive. Active analytical redundancy consists of fault separation, controller reconfiguration, and detection. This complex, resource-heavy, and slow operating system can work around many different kinds of bugs, which is its main advantage. Passive analytical redundancy is a fast and easy strategy since it relies on a robust controller design that can handle only uncertainties and defects in a system. It can't deal with many different kinds of flaws [4].

The most crucial component of an AFTCS is the Fault Detection and Isolation (FDI) unit, which is in charge of identifying issues with actuators and sensors. The FDI unit is made possible by the creation of an observer model that generates approximation values in the case of a failed component. When an error is found and fixed, the FDI adjusts the controller's settings in accordance with the observer's predictions of the relevant parameters in light of the new context. Although it can identify a broad variety of faults in real time, AFTCS is computationally demanding, sluggish, and difficult to use [5].

The state space modeling of AFTCS to implement observer-based architecture is explained in [4] in which a residual is calculated by subtracting observer value from the actual value. If the residual goes to zero, no fault is declared by the FDI unit. Fault is declared if the residual goes out of the threshold. For our problem, there is an added complexity due to nonlinearity in VFDs. Therefore, nonlinear observer design was performed as our problem needs. The design of the observer for a nonlinear system was adopted from [6] as follows:

$$\dot{\bar{x}}(t) = A\bar{x}(t) + Bu + g(\bar{x},\ u, t) + \bar{L}\left(C\bar{x} - y\right) \tag{1}$$

Let $e_x(t)$ represents the error vector

$$e_x(t) \hat{=} \bar{x}(t) - x(t)$$

We can obtain its derivative as:

$$\dot{e}_x = \left(A + \bar{L}C\right) e_x(t) + \left(g(\bar{x},\ u, t) - g(x,\ u, t)\right) \tag{2}$$

The error e_x must converge to zero asymptotically for stability. The stability condition is ensured using the second Lyapunov stability criterion for nonlinear systems [7]. Schur complement will also be used for matrix simplifications [8].

Lemma 1: *For error $e_x(t)$ asymptotically to approach to zero, let's assume there exists a matrix R, X, and scalar μ to satisfy the following linear matrix inequality such that $= R^T > 0$ and $\mu > 0$:*

$$\begin{bmatrix} RA + A^TR + XC + C^TX^T + \ \mu\lambda^2 I & R \\ R & -\mu I \end{bmatrix} < 0 \tag{3}$$

And the gain matrix of the observer:

$$\bar{L} = R^{-1}X \tag{4}$$

Lyapunov function:

$$V(t) = e_x^T R e_x(t) \tag{5}$$

$$\begin{aligned} \dot{V} &= e_x^T \left(RA + R\bar{L}C + A^TR + C^TL^{-T}R\right) e_x \\ &+ 2e_x^TR\left(g(\bar{x},\ u, t) - g(\ x,\ u, t)\right) \\ &\le e_x^T \left(RA + R\bar{L}C + A^TR + C^TL^{-T}R\right) e_x + {}^1\!/_{\mu} e_x^T R^2 e_x \\ &+ \mu \| g(\bar{x},\ u, t) - g(\ x,\ u, t) \|^2 \\ &\le e_x^T (RA + R\bar{L}C + A^TR + C^TL^{-T}R) e_x \\ &+ {}^1\!/_{\mu} e_x^T R^2 e_x + \mu\ \lambda^2 \|e_x\|^2 \end{aligned}$$

$$= e_x^T(RA + R\bar{L}C + A^TR + C^TL^{-T}R + \mu\ \lambda^2 I + {}^1\!/_{\mu}R^2)e_x \tag{6}$$

Substituting the Eq. (4) into the above equation to get:

$$\dot{V} \le e_x^T\left(RA + XC + A^TR + C^TX^T + \mu\ \lambda^2 I + {}^1\!/_{\mu}R^2\right)e_x \tag{7}$$

If the following inequality holds, e_x converges asymptotically to zero.

$$RA + XC + A^TR + C^TX^T + \mu\ \lambda^2 I + {}^1\!/_{\mu}R^2 < 0 \tag{8}$$

Theorem 1: *For error $e_x(t)$ to approach zero exponentially with rate $\kappa/2$ lets assume matrices R, X and scalars μ, κ to satisfy the following such that $R = R^T > 0$ and $\mu, \kappa > 0$:*

$$\begin{bmatrix} RA + A^TR + XC + C^TX^T + \ \mu\lambda^2 I + \kappa R & R \\ R & -\mu I \end{bmatrix} < 0 \tag{9}$$

where

$$\bar{L} = R^{-1}X \tag{10}$$

$$\dot{V}(t) \le -\kappa e_x^T R e_x = -\kappa V(t) \tag{11}$$

Hence, we get

$$V(t) \le e_x^T V(0) \tag{12}$$

$$\lambda_{min}(R)\,\|e_x(t)\|^2 \le e^{-kt}\lambda_{max}(R)\,\|e_x(0)\|^2 \tag{13}$$

Where $\lambda_{min} and \lambda_{max}$ are minimum and maximum Eigenvalues of matrix R respectively. Hence, we obtain the following norm of the error vector:

$$\|e_x(t)\| \le \sqrt{{}^{\lambda_{max}(R)}\!/_{\lambda_{min}(R)}}\|e_x(0)\|e^{-kt/2} \tag{14}$$

The residual equation can be obtained as:

$$r(t) \ \hat{=}\ \|C\bar{x}(t) - y(t)\| \tag{15}$$

$$r(t) \le \sqrt{{}^{\lambda_{max}(R)}\!/_{\lambda_{min}(R)}}\|C\|\|e_x(0)\|e^{-\frac{kt}{2}} \tag{16}$$

Hence, for fault detection of sensor fault, we have the following criteria

$$r(t)\begin{cases} \le \sqrt{{}^{\lambda_{max}(R)}\!/_{\lambda_{min}(R)}}\ \|r(0)\|\ e^{-\frac{kt}{2}}, \\ \qquad\qquad there\ is\ no\ fault \\ > \sqrt{{}^{\lambda_{max}(R)}\!/_{\lambda_{min}(R)}}\ \|r(0)\|\ e^{-\frac{kt}{2}}, \\ \qquad\qquad there\ is\ a\ fault \end{cases} \tag{17}$$

Hardware redundancy approaches may be categorized into two main types: dual redundancy and triple modular redundancy. To accomplish the same task, the DR design incorporates both the main and secondary components. When one part of a system fails, the secondary part steps in to keep operations running smoothly [9].

Further contents of the paper are organized as: literature review is described in Section 1.2, methodology in Section 2; results and discussion in Section 3; reliability analysis in Section 3.3; and comparison in Section 3.4. Finally, the article is concluded in Section 4.

1.2. Literature review

Using the maximum likelihood voting method, Kalman filter, and adaptive observer, this paper presents a design for an IM drive that can withstand mechanical sensor failure. A reliable and easy-to-understand method for fault diagnostics in drive systems for three-phase induction motors was presented by the authors in [10]. Referenced in [11] is an extensive explanation of a fault-tolerant control system for a high-performance induction motor drive in a vehicle. Once a sensor stops working, the suggested system modifies its control methods.

To identify and find powertrain problems in electric vehicles, the authors of [12] detailed the most recent fault diagnostic methods. Defects, whether mechanical or electrical, were the main emphasis. There may be one or more of them. It is critical to have accurate and consistent sensor measurement data for DTC to be safe. This research [13] proposes a paradigm shift toward fault-tolerant control based on a dual-torque model. By adding the stator current vector, stator flux vector, and their scalar and vector products to a new state variable, it is possible to construct a novel dual-torque model of an induction motor. After that, a current observer is added to this model so that it may be controlled in a fault-tolerant dual-torque approach. An intriguing area of study has been the capability of multiphase induction motor (IM) drives to withstand faults without requiring additional hardware, as discussed in [14]. To approximate the rotor position, the technique makes use of a mathematical

model of the motor drives in conjunction with the windings' instantaneous currents and voltages. One possible way to prevent open-circuit failures is to inject zero-sequence compensation voltage feedforward, as shown in the article [15]. Unlike previous feedforward fault-tolerant control systems, the suggested method does not need the collection of data on the magnetizing inductance—something that might be challenging with induction motors. To find and diagnose faulty switches, FDI in the research [16] uses artificial neural networks (ANN). As a precaution, the switches supposedly include two sets of redundant hardware. A load-side fault detector was built that uses ANN to identify when anything goes wrong from the outside.

A comprehensive description of the development of FTCS employing cutting-edge machine learning techniques is given in the article [17]. Two methods for diagnosis are proposed in the article [18]: total harmonic distortion (THD) and a normalized output voltage factor calculation. Including FDI units in the enlarged fault-tolerant design greatly improved reliability and decreased THD to around 18%, as shown in the simulation results. The purpose of this research was to use computer simulations to find ways to lessen the impact of variations in load and speed [19]. A fault-tolerant control system based on a current sensor is detailed in [20] for a direct rotor flux-oriented induction motor drive.

An FTC system for three-phase induction motor drives is suggested by the authors of [21]. This system would use current sensors rather than speed sensors. Standard practice dictates the usage of an open-loop speed estimator-based sensorless FOC system. The task of FDI is carried out by a third-difference operator. In the event of a malfunction after FDI, a sensorless FOC technique based on the extended Kalman filter is used. There is extensive research on the process of identifying an electrical issue with a speed controller in MCUS in the publication [22]. This study combines the model-based sliding mode approach with the signal-based Power Inverter Voltage fail detection methodology to provide FTC for sensorless speed. Controlling a permanent magnet synchronous motor. Some of the most prevalent kinds of problems in industrial drive systems are open-circuit failures in the stator windings of Three-Phase Induction Machines (TPIMs). In the event of an open-circuit failure, the article [23] aims to provide a summary of the techniques presently used to control TPIM drives. Magneto-motive force, transformation matrices, and harmonic injection are the three main categories under which these control methods fall. For DC motors that are stimulated individually, the authors of [24] detail triple modular redundancy and very redundant switching systems. The proposed method may be able to continue producing from the working switch even if two of them are damaged. In addition to covering FDD techniques, this article [25] neatly sorts defects into four groups: machine, power electronics, DC link capacitor, and sensor. Statistics, machine learning, and deep learning are the three main categories of FDD methods used on computers. To protect robust smart systems from denial-of-service assaults, [26] suggests a blockchain-based solution. A microgrid system based on PI controllers is the subject of investigation from many sites.

A comprehensive analysis of the many inverter failure modes and their detection techniques is presented in the review paper [27]. The study [28] presents solutions for advanced stationary frame voltage control in current source inverters (CSI) with linear and nonlinear loads, respectively, to achieve zero steady-state error. These approaches are based on the mathematical model of the CSI in the stationary $\alpha\beta$ frame. Using the Instantaneous Power Theory for multiphase AC systems as a foundation, [29] constructs an analytical model of the DC-link voltage oscillations to deduce their source. For every kind of failure and every kind of operating location, the suggested control approach with a peak current limiter eliminates the double-fundamental frequency oscillations in the DC-link.

The main contribution of this paper is the design of an AFTCS for the speed sensor, current sensors, and switch faults in the inverter module. An estimated value for open loop speed estimation is used for the speed sensor with the help of flux estimation. The fault tolerance of the current sensors is achieved such that to replace the defective value with the average value of the other two functional current sensors in the event of a failure in one sensor assuming that only one sensor gets faulty at a time. Moreover, the FDI unit can detect a defective switch and replace it with a backup redundant switch in the shortest possible timeframe. The stability and convergence of the observer is also proved using the Lyapunov theorem. The use of Markov chains in the analysis of reliability further confirmed the system's outstanding reliability. To assess the efficiency of the proposed method, a variable-speed system is built for an induction motor with a power capacity of 1.1kW using MATLAB/Simulink. The system is deployed on an STM32-Nucleo-F103RB board with hardware-in-the-loop functionality to verify the precision of the simulation outcomes. Furthermore, a thorough analysis was conducted to demonstrate the enhanced efficiency and increased reliability of the suggested model in comparison to the existing literature.

2. Materials and methods

2.1. Types of faults in drive systems

The major components of drive systems that are prone to failures are the Machine (or Motor), Converter, Sensors or sensing unit, and control unit. Some common types of faults include [30]:

1. Stator Faults: These include short circuits or open circuits in the stator windings, which can lead to unbalanced currents, reduced torque production, and overheating of the motor.
2. Rotor Faults: Rotor faults can manifest as broken rotor bars or end rings, resulting in torque pulsations, increased vibrations, and reduced motor efficiency.
3. Power Electronics Faults: Faults in power electronic components, such as inverters or converters, can cause voltage or current distortions, leading to improper motor operation or even complete motor failure.
4. Sensor Faults: Sensor faults, such as failures in speed or position sensors, can result in inaccurate measurements, leading to degraded motor control performance.

2.2. Modeling of three-phase induction motor

The mathematical modeling of a TPIM can be described as (18)–[27] in the dq stationary reference frame (SRF) [11]:

Voltage equations for stator d-axis and q-axis:

$$v_{ds}^{s} = r_s I_{ds}^{s} + p\varphi_{ds}^{s} \tag{18}$$

$$v_{qs}^{s} = r_s I_{qs}^{s} + p\varphi_{qs}^{s} \tag{19}$$

Voltage equations for rotor d-axis and q-axis:

$$v_{dr}^{s} = 0 = r_r I_{dr}^{s} + p\varphi_{dr}^{s} + \Omega_r \varphi_{qr}^{s} \tag{20}$$

$$v_{qr}^{s} = 0 = r_r\, I_{qr}^{s} + p\varphi_{qr}^{s} - \Omega_r \varphi_{dr}^{s} \tag{21}$$

Flux equations for stator d-axis and q-axis:

$$\varphi_{ds}^{s} = L_s I_{ds}^{s} + L_m I_{dr}^{s} \tag{22}$$

$$\varphi_{qs}^{s} = L_s I_{qs}^{s} + L_m I_{qr}^{s} \tag{23}$$

Flux equations for rotor d-axis and q-axis:

$$\varphi_{dr}^{s} = L_m I_{ds}^{s} + L_r I_{dr}^{s} \tag{24}$$

$$\varphi_{qr}^{s} = L_m I_{qs}^{s} + L_r I_{qr}^{s} \tag{25}$$

Torque equation:

$$T_e = \frac{\text{pole}}{2}\left(L_m I_{qs}^{s} I_{dr}^{s} - L_m I_{ds}^{s} I_{qr}^{s}\right) \tag{26}$$

Motion equation:

$$T_e - T_l = \frac{2}{\text{pole}}\left(Jp\Omega_r + F\Omega_r\right) \tag{27}$$

In (18) to (27), superscript "*s*" indicates the variables in the SRF domain. Stator and rotor *dq* voltages are shown by v_{ds}^{s}, v_{qs}^{s}, v_{dr}^{s}, v_{qr}^{s}. Stator and rotor resistances: r_s, r_r and stator and rotor self- and mutual inductances: L_s, L_r, L_m ($L_s = L_{ls} + L_m$ and $L_r = L_{lr} + L_m$). Stator and rotor *dq* fluxes are shown by φ_{ds}^{s}, φ_{qs}^{s}, φ_{dr}^{s}, φ_{qr}^{s}. Stator and rotor *dq* currents are represented by I_{ds}^{s}, I_{qs}^{s}, I_{dr}^{s}, I_{qr}^{s}. Stator and rotor leakage inductances: L_{ls}, L_{lr}. Electromagnetic torque and load torque: T_e, T_l. Electrical motor angular speed: Ω_r. p represents the differential operator. *Pole*, *F, and J* represent the number of poles, viscous friction coefficient, and moment of inertia respectively.

2.3. Open-loop speed estimator

In this paper, an open-loop method is used for the estimation of speed during normal mode. The *dq* voltages and currents are used using the rotor *dq* currents on the model of 3-PIM as (28) and (29):

$$I_{dr}^{s} = \frac{1}{I_m}\int \left(v_{ds}^{s} - r_s I_{ds}^{s} - I_s p I_{ds}^{s}\right) \mathrm{d}t \tag{28}$$

$$I_{dr}^{s} = \frac{1}{I_m}\int \left(v_{ds}^{s} - r_s I_{ds}^{s} - I_s p I_{ds}^{s}\right) \mathrm{d}t \tag{29}$$

The current sensors provide values of *dq* currents and the controller provides the values of *dq* voltages. According to (18) to (29) the speed can be estimated as Eq. (30):

$$\hat{\Omega}_{r1} = \frac{1}{I_m I_{qs}^{s} + I_r I_{qr}^{s}}\left(-I_m p I_{ds}^{s} - r_r I_{dr}^{s} - I_r p I_{dr}^{s}\right) \tag{30}$$

where superscript "^" represents the estimated values. In addition, $\hat{\Omega}_{r1}$ is the estimated speed obtained from the open-loop speed estimator. In Eq. (30), when $I_m I_{qs}^{s} + I_r I_{qr}^{s} = \varphi_{qr}^{s} = 0$, the denominator of this equation becomes zero. In this condition, the speed can be estimated based on (30)

$$\hat{\Omega}_{r1} = \frac{r_r I_{qr}^{s} + p I_{qr}^{s}}{\varphi_{dr}^{s}} \tag{31}$$

The open-loop speed estimator has a lower computational complexity than the other estimators;

nevertheless, it has a few downsides, such as dependent parameters and poor accuracy. The performance of the open-loop speed estimator is subpar at very slow speeds and in circumstances that are just temporary. Problems like saturation and offset might arise since this approach necessitates integrations and differentiations. This study aims to reduce control system complexity by studying a speed estimate approach based on open-loop operation for pre-fault drive system functioning.

2.4. Sensorless FOC strategy

During the pre-fault procedure, this strategy is used in the present examination. Keep in mind that this study assumes the drive mechanism won't work inside the field weakening range. Superscript "e" designates the variables in the rotating reference frame (RRF). While there are many benefits of sensorless FOC, such as increased dependability and lower costs, there are also some drawbacks, such as potential accuracy issues and challenges with algorithm design, particularly at low speeds or in dynamic settings.

The *dq* voltages of 3-PIM are calculated using two current sensors (phase "*a*" and phase "*b*") and the estimated value of speed in the RRF (v^e_{ds}, v^e_{qs}). A pulse width modulation (PWM) switching method is used in the 3-phase VSI using *abc* voltages to generate six pulses.

$$\begin{bmatrix} I^s_{ds} \\ I^s_{qs} \end{bmatrix} = \sqrt{\frac{2}{3}} \begin{bmatrix} 1 & -0.5 & -0.5 \\ 0 & \frac{\sqrt{3}}{2} & -\frac{\sqrt{3}}{2} \end{bmatrix} \begin{bmatrix} I_{as} \\ I_{bs} \\ I_{cs} \end{bmatrix} \tag{32}$$

$$\begin{bmatrix} I^e_{ds} \\ I^e_{qs} \end{bmatrix} = \begin{bmatrix} \cos\alpha_e & sin\ \alpha_e \\ -sin\ \alpha_e & \cos\alpha_e \end{bmatrix} \begin{bmatrix} I^s_{ds} \\ I^s_{qs} \end{bmatrix} \tag{33}$$

$$\begin{bmatrix} v_{as} \\ v_{bs} \\ v_{cs} \end{bmatrix} = \sqrt{\frac{2}{3}} \begin{bmatrix} 1 & -0.5 & -0.5 \\ 0 & \frac{\sqrt{3}}{2} & -\frac{\sqrt{3}}{2} \end{bmatrix}^T \begin{bmatrix} v^s_{ds} \\ v^s_{qs} \end{bmatrix} \tag{34}$$

$$\begin{bmatrix} v^s_{ds} \\ v^s_{qs} \end{bmatrix} = \begin{bmatrix} \cos\alpha_e & -sin\ \alpha_e \\ sin\ \alpha_e & \cos\alpha_e \end{bmatrix} \begin{bmatrix} v^e_{ds} \\ v^e_{qs} \end{bmatrix} \tag{35}$$

In (32) to (35), v_{as}, v_{bs}, v_{cs}, I_{as}, I_{bs}, I_{cs} are stator voltages and currents ($I_{cs} = -I_{as} - I_{bs}$).

2.5. FDI mechanism

To start, the algorithm takes the RMS current values from each switch and passes them into the input, as shown in Fig. 2. Following a 0.2-second transverse delay, the fault detection block engages the redundant S1 switch to replace the broken one. As the switch is swapped over in microseconds, a little delay is provided in the simulation circuit to enhance viewing just like a practical scenario.

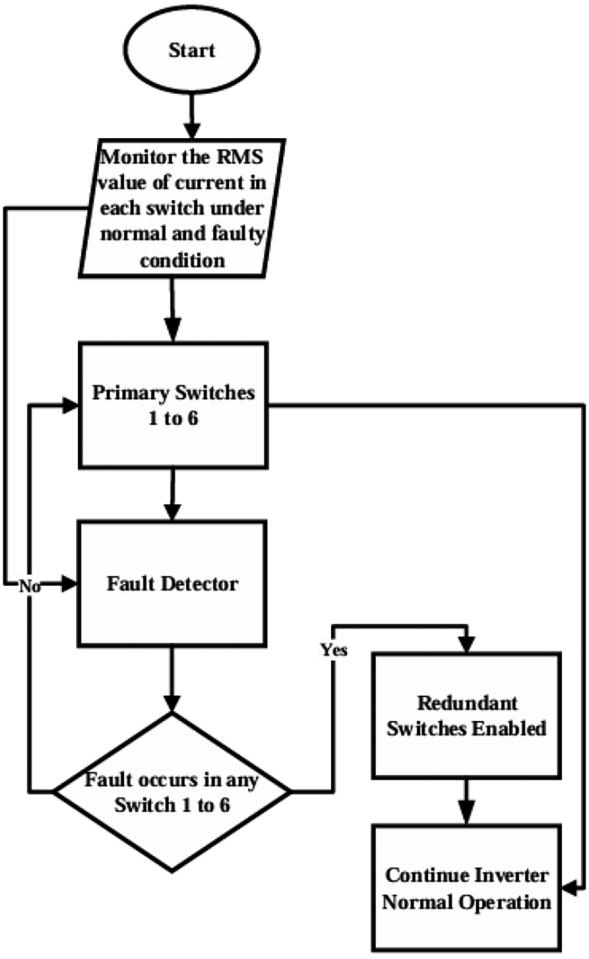

Fig. 2. Flowchart of proposed switch fault tolerance.

Any other switch will also use the same technique. If a switch goes out, its secondary switches will kick in, reducing the current through the faulty switch to almost nothing and the voltage approaching the supply voltage.

Implementing the suggested fix will prevent the switch failure from affecting the system's functionality. When the main and backup parts quit functioning, the system will fail. Durability, efficiency, and dependability are all enhanced by the suggested repair. Once the system is started, the input parameters are simulated. In the FTI architecture, you can find nine switches that can be turned between two states. When any of the six primary switches fail, the FDI unit will identify the issue and use the backup switches to run the IMD until the damaged switches are replaced.

This method has the drawback of only triggering system failure if both the main and redundant components fail. The planned DHR FTC would make the hardware system bulkier and more expensive. While

closed, switches should have infinite resistance; when open, they should have zero. Actually, when closed, switches often create a little delay with high resistance, and when open, they typically generate moderate resistance. It is also necessary to have an FTC on the load side.

2.6. Simulation circuit

The proposed fault-tolerant induction motor drive (FTIMD) has been developed with a vector space vector control algorithm using redundant IGBT switches, as shown in Fig. 3.

The model consists of individual subunits as follows:

1. Vector Control Block
2. Fault Injection Unit (FIU) Control block
3. SVPWM Block
4. Fault Detector Units Block
5. Fault-Tolerant Inverter Module
6. Induction Motor Block
7. Speed Sensor Fault Tolerance Block

The model is developed for fault tolerance against faults in the current sensors, speed sensors, and IGBT switches in the inverter module. This makes the proposed IMD model highly reliable and robust. This is to mention that little performance degradation takes place in the events of faults, however, the system maintains stability thereby avoiding shutdown and production loss.

The faults are injected using the FIU, in which the control of 6 IGBT switches, current sensors, and speed sensors are shown. The fault is injected by pressing the slider switch to the Fail position. The indication displays green in normal conditions and becomes red in faulty conditions. This unit injects the binary faults into the system. The FIU issues the order to the block. The FDI unit receives a value of 1 when the switch is functioning properly and a value of 0 when the switch is malfunctioning.

The standby switch takes place when a fault is injected through the FIU unit. The fault detection and switching function is performed by the FDI unit. Two independent IGBT outputs—one from the main IGBT and one from the backup—are controlled by this system. During regular operation, the typical IGBT provides the output to the power circuit. The faulty switch is located and disconnected in the case of a malfunction. The standby switch's output is then, realistically, transmitted to the power circuit after a little delay. There are two indications on the FDI unit's fault detection unit. In the first scenario, a continuous zero signal block occurs because the redundant IGBT is disabled while the main IGBT is

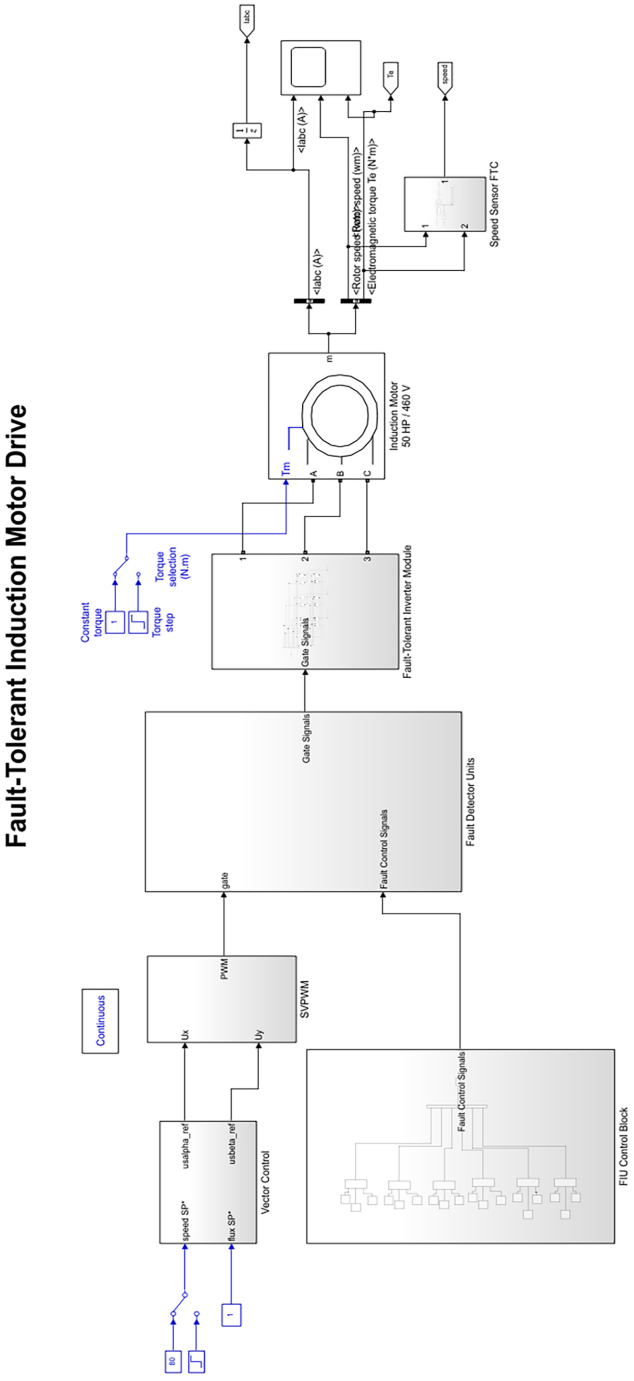

Fig. 3. Proposed FTIMD model.

in operation. A healthy signal is what activates the main IGBT. In addition to injecting a fault signal, the fault control signal applies a gate signal to redundant IGBTs, isolating the problematic one simultaneously.

The fault tolerance for the current sensor is implemented. The faulty current sensor value is replaced by the average value of the other two healthy current sensors thereby preventing the drive shutdown due to current sensors failure. This research assumes

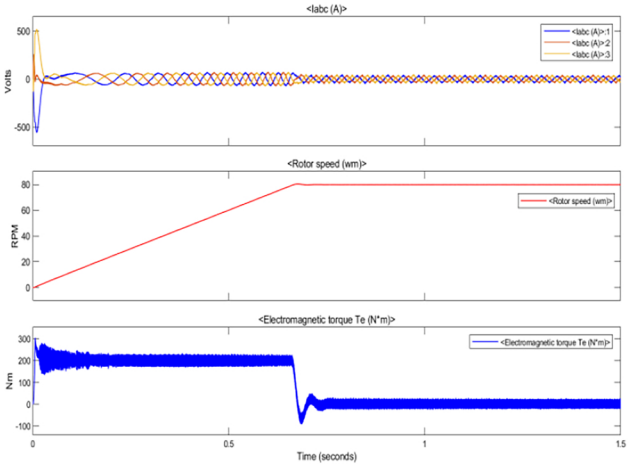

Fig. 4. Voltage, speed, and torque waveforms in normal conditions.

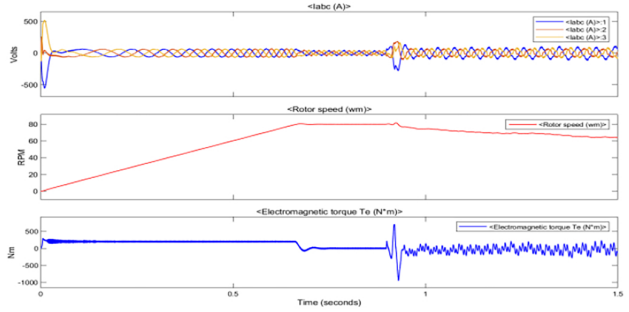

Fig. 5. Voltage, speed, and torque waveforms in current sensors faulty conditions.

that switching between IGBTs takes exactly zero time. Hardware redundancy increases the whole system's physical dimensions, weight, complexity, and expense, which is one of the work's drawbacks. If the two backup switches go down simultaneously, the proposed method will not work and the system will power down. It is also assumed that ideal switches have zero resistance when closed and infinite resistance when open. In contrast, their closed resistance is low and their finite resistance is considerable when they are in the open condition.

3. Results and discussions

3.1. Simulation results

3.1.1. Normal behaviour

The output results of the three-phase input voltages to the drive, motor speed RPM, and the output torque in normal working conditions without any fault, are shown in Fig. 4.

3.1.2. Fault tolerance for current sensors

The fault tolerance results for the current sensors are shown in Fig. 5. In case of a fault in one current

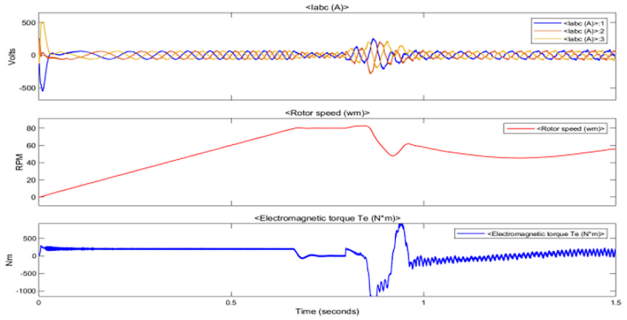

Fig. 6. Voltage, speed, and torque waveforms in speed sensor faulty conditions.

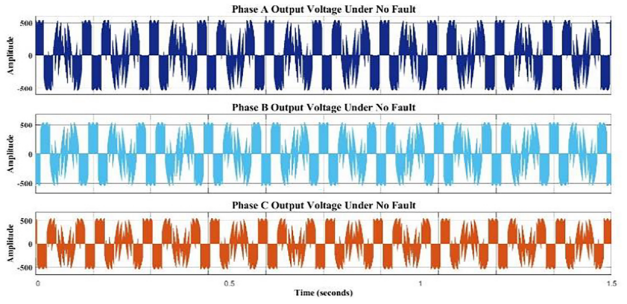

Fig. 7. Three-phase output voltage of FTI under no fault condition.

sensor, the faulty value is replaced by the average value of the other two healthy current sensors. It is assumed that only one current sensor fails at a time, simultaneous faults in more than one current sensor are not considered in this research.

3.1.3. Faults tolerance for speed sensor

The fault tolerance results for the speed sensor are shown in Fig. 6. AFTCS has been implemented for speed sensor to identify the sensor fault and replace the faulty value with an estimated value as explained in Section 3 for open loop speed estimation using flux estimation based observer.

3.1.4. Fault tolerance for inverter switches

The normal three-phase output produced by the FTI is shown in Fig. 7.

At 0.1 seconds, the fault is injected by the FIU, and the resulting output waveform is shown in Fig. 8. After a brief interruption during fault injection, the output returns to normal functioning when the faulty switch is replaced with the dependable standby IGBT switch, as shown in the results. Fig. 8 shows that in the event of a failure, the voltage of one of the phases will oscillate between zero and thirty-three seconds until the mistake is corrected by the redundant components.

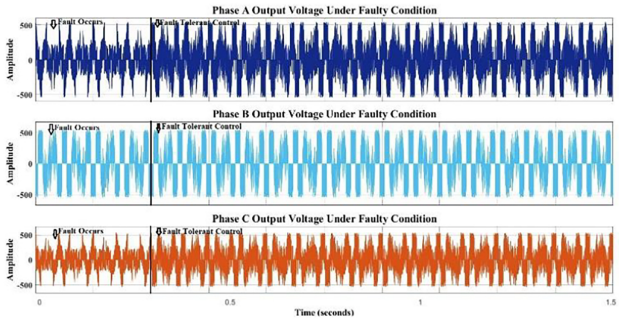

Fig. 8. Output voltage of each phase of FTI under faulty condition.

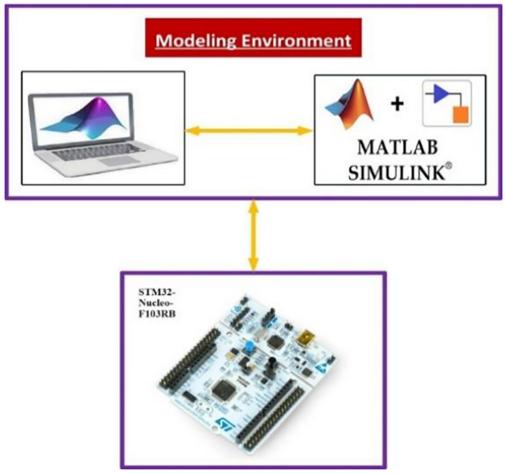

Fig. 9. Hardware-in-the-loop setup.

3.2. Hardware-in-the-loop

The setup of the HIL experiment is shown in Fig. 9. A connection connects the PC to the STM32-Nucleo-F103RB microcontroller. The purpose of the HIL experiment is to verify and evaluate the suggested controller's functionality in an actual setting. In terms of dynamic behavior, the suggested controller is identical to that of the simulation findings.

When working with hardware in MATLAB/Simulink, you have three options: External Mode for building, deploying, and starting; Connected Input Output; and EM for monitoring and tuning. To confirm the above-mentioned simulation findings, the switch failure is implemented utilizing hardware-in-the-loop.

To put the model into hardware and configure it, you may utilize the EM monitor and tweak the configuration mode. Referring to Fig. 10, choose the hardware board and com-port that the STM32 is attached to.

Automatic generation and burning of C code onto the hardware board occurs upon model viewing and modification. The simulation and hardware

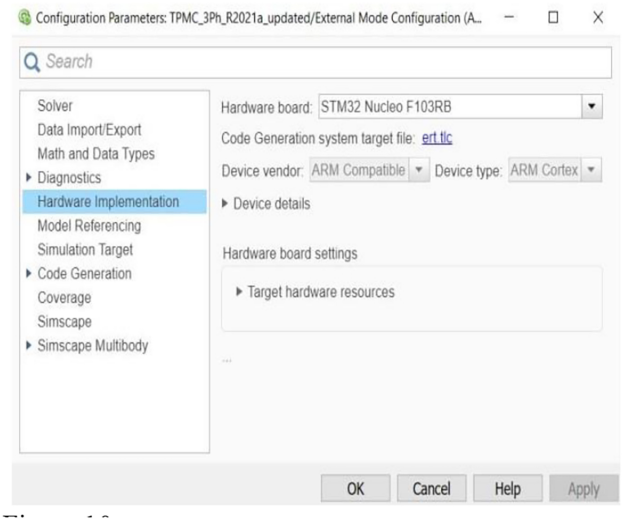

Fig. 10. Hardware implementation settings.

findings are in agreement for all fault scenarios including speed sensors, current sensors, and inverter switches.

To make the system more reliable and resilient, the DHR should be used. Simultaneously add a copy of the primary and secondary components in DHR. The system continues to function thanks to the redundant component, which kicks in in the case of the primary component failure. If both the primary and secondary parts of the system break down, the whole thing will not work. To manage switching operations, the FTI design makes use of six bidirectional switches, S1–S6. In conjunction with the other switches, the other six redundant switches, S1 through S6, are employed in duplicate. Two IGBTs and two freewheeling diodes are included in each switch. The DHR system was installed to prevent the system from powering down in the event of a switch malfunction. The problem has been identified and is being handled by the FDI section. The backup component is activated to avoid shutdowns in the very improbable case that the main component fails. Given the imperfect circumstances, the suggested action is the most effective one.

3.3. Reliability analysis

Since fault tolerance is introduced in the inverter block using hardware redundancy, the reliability analysis can be made using Markov chains. Mean Time to Failure (MTTF) is a crucial quantitative metric for evaluating the reliability of a system. The MTTF is the typical interval between predicted failures of a given item. For MTTF modeling to work, the broken object must either have an indefinite repair time or be completely unfixable. Here is the formula

that is used to calculate the MTTF:

$$MTTF = \int_0^\infty R(t)\,dt \tag{36}$$

MTTF can also be calculated by taking the reciprocal of failure rate (λ) as follows:

$$MTTF = \frac{1}{\lambda} \tag{37}$$

For the inverter module in the FTIMD system, we get

$$\lambda_1 = (2N-1)\,\lambda_0 \tag{38}$$

where λ_0 is the failure rate of a single IGBT switch. By differentiation, we get

$$\frac{dP_1}{dt} = -2\lambda_1 P_1(t) \tag{39}$$

Hence,

$$R(t) = P_1(t) = e^{-2(2N-1)\lambda_0 t} \tag{40}$$

where N represents the number of switch modules in the MLI. Without fault tolerance, we get

$$MTTF_{without\ FTC} = \frac{1}{2\lambda_0}\left(\frac{1}{2N-1}\right) \tag{41}$$

$$\lambda_1 = \left(\frac{2N-1}{2}+1\right)\lambda_0 \tag{42}$$

The failure rate of the two modules would be as follows:

$$\lambda_2 = \left(\frac{2N-1}{2}\right)\lambda_0 \tag{43}$$

From Markov chains, we get

$$\frac{dP_1}{dt} = -\lambda_1 P_1(t) \tag{44}$$

$$P_1(t) = e^{-\left(\frac{2N-1}{2}+1\right)\lambda_0 t} \tag{45}$$

$$\frac{dP_1}{dt} = \lambda_1 P_1(t) - \lambda_2 P_2(t) \tag{46}$$

$$P_2(t) = \left(\frac{2N-1}{2}\right)\left(e^{-\left(\frac{2N-1}{2}\right)\lambda_0 t} - e^{-\left(\frac{2N-1}{2}+1\right)\lambda_0 t}\right) \tag{47}$$

The total reliability would be as follows:

$$R(t) = P_1(t) + P_2(t) = \left(\left(\frac{1-2N}{2}\right)e^{-\left(\frac{2N-1}{2}+1\right)\lambda_0 t}\right) + \left(\frac{2N-1}{2}\right)\left(e^{-\left(\frac{2N-1}{2}\right)\lambda_0 t}\right) \tag{48}$$

$$MTTF_{with\ FTC1} = \frac{1}{\lambda_0}\left(\frac{1-N}{N+1}\right) \tag{49}$$

$$\lambda_2 = (2N-3)\,\lambda_0 \tag{50}$$

$$\frac{dP_1}{dt} = -(\lambda_1+\lambda_2)P_2(t) - \lambda_1 P_1(t) \tag{51}$$

$$P_2(t) = \left(\frac{2N-3}{2}\right)\left(e^{-(\lambda_1+\lambda_2)t} - e^{-2\lambda_1 t}\right) \tag{52}$$

$$\frac{dP_4}{dt} = -(2\lambda_2)P_4(t) + \lambda_1 P_2(t) + \lambda_1 P_3(t) \tag{53}$$

$$P_4(t) = \frac{(2N-3)^2}{4}\left(e^{-2\lambda_1 t} + e^{-2\lambda_2 t}\right) - \frac{(2N-3)^2}{2}e^{-(\lambda_1+\lambda_2)t} \tag{54}$$

$$R(t) = P_1(t) + P_2(t) + P_3(t) + P_4(t) \tag{55}$$

$$R(t) = \left((2N-2) + \frac{(N-3)^2}{4}\right)e^{-2(2N-1)\lambda_0 t} + \left((2N-3) + \frac{(2N-3)^2}{4}\right)e^{-2(2N-2)\lambda_0 t} + \left(\frac{(2N-3)^2}{4}\right)e^{-2(2N-3)\lambda_0 t} \tag{56}$$

$$MTTF_{with\ FTC} = \frac{1}{2\lambda_0}\left(\frac{\left((2N-2)+\frac{(2N-3)^2}{4}\right)}{(2N-1)} + \frac{\left((2N-3)+\frac{(2N-3)^2}{4}\right)}{(2N-2)} + \frac{\left(\frac{(2N-3)^2}{4}\right)}{(2N-3)}\right) \tag{57}$$

The equation demonstrates that the MTTF has significantly increased with the proposed fault tolerance architecture.

3.4. Comparison with existing works

To prove its improved performance, the suggested FTIMD has been compared in this part and the results are provided in Table 1. The authors provide a paradigm for fault-tolerant control based on a dual-torque model in their paper [11]. By selecting a different state variable, they were able to construct a new dual-torque model of an induction motor that incorporates the scalar product and vector product of the stator current vector and stator flux. Then, this model is coupled with an existing observer to provide

Table 1. Comparison of proposed work with previous works.

Component	Reference [13]	Reference [21]	Proposed Work
Hardware Redundancy	No	No	Yes
Speed Sensor Fault Tolerance	Dual-torque model	Extended Kalman Filter	Open Loop Sensorsless Control
Current Sensors Fault Tolerance	No	No	Yes
Control Complexity	Very Complex	Very Complex	Relatively Simple

a fault-tolerant dual-torque model control approach. An FTC for three-phase induction motor drives was suggested in [21] that would use current sensors rather than speed measurements. An open-loop speed estimator-based sensorless FOC approach was built for use in typical applications. For FDI, the task of defect identification and isolation falls on a third-difference operator. The sensorless FOC approach was built on an extended Kalman filter to address the issue following FDI.

4. Conclusion

This paper presented a unique fault tolerance strategy that enables the construction of highly reliable induction motor drives with hardware and analytical redundancies. The architecture was designed to ensure redundancy in the case of failures in the current sensors, IGBT switches, or speed sensors of the inverter module. A dedicated FDI device has been created with the particular purpose of identifying and isolating the defective switch, allowing for the subsequent implementation of a backup redundant switch. AFTCS was employed with a flux estimation-based observer to identify instances of speed sensor malfunction and then used the estimated values to substitute the defective ones in the open-loop speed estimates. The fault tolerance of the current sensors was designed such that to replace the defective value with the average value of the other two functional current sensors in the event of a failure in one sensor assuming that only one phase current sensor gets faulty at a time. The stability and convergence of the observer were also proved using the Lyapunov theorem. A 1.1 kW induction motor variable-speed system was constructed using MATLAB/Simulink to test the suggested technique. The study on reliability, using Markov chains, provided more empirical support for the system's enhanced dependability. A comparative analysis was also undertaken to illustrate the improved performance and heightened dependability of the proposed work in relation to existing literature.

Future research directions may include the design of a more sophisticated estimation algorithm with machine learning techniques in the AFTCS design for more accurate fault diagnosis and tolerance. The engineering values such as rise time or the settling time for comparison with past works may also be considered.

Conflict of interest

The authors declare no conlict of interest

Author contribution

Conceptualization, Z.A.A.; Formal analysis, Z.A.A.; Funding acquisition, Z.A.A.; Investigation, Z.A.A.; Methodology, Z.A.A.; Project administration, Z.A.A.; Resources, Z.A.A.; Software, Z.A.A., Supervision, Z.A.A.; Validation, Z.A.A.; Visualization, Z.A.A.; Writing—original draft, S.W.; Writing—review & editing, Z.A.A.

Data availability

No datasets were generated or analyzed during the current study.

List of abbreviations

Abbreviation	Description
EVs	Electric Vehicles
DHR	Dual Hardware Redundant
FOC	Field-Oriented Control
DTC	Direct Torque Control
FTC	Fault-Tolerant Control
AFTCS	Active Fault-Tolerant Control System
FDI	Fault Detection And Isolation
IM	Induction Motor
TPIMs	Three-Phase Induction Machines
THD	Total Harmonic Distortion
ANNs	Artificial Neural Networks
RRF	Rotating Reference Frame
MTTF	Mean Time to Failure

References

1. Yang Z, Shang F, Brown IP, Krishnamurthy M. Comparative study of interior permanent magnet, induction, and switched reluctance motor drives for EV and HEV applications. IEEE Transactions on Transportation Electrification. Oct. 2015;1(3):245–254. doi: 10.1109/TTE.2015.2470092.

2. Nikpayam M, Ghanbari M, Esmaeli A, Jannati M. Fault-tolerant control of Y-connected three-phase induction motor drives without speed measurement. Measurement. Jan. 2020;149:106993. doi: 10.1016/j.measurement.2019.106993.
3. Ji Z, Zhao J, Sun Y, Yao X, Zhu Z. Fault-tolerant control of cascaded H-bridge converters using double zero-sequence voltage injection and DC voltage optimization. Journal of Power Electronics. 2014;14(5):946–956.
4. Amin AA, Hasan KM. A review of fault tolerant control systems: Advancements and applications. 2019. doi: 10.1016/j.measurement.2019.04.083.
5. Stengel RF. Intelligent failure-tolerant control. IEEE Control Systems Magazine. 1991;11(4):14–23.
6. Wang Y, Zhou D, Joe Qin S, Wang H. Active fault-tolerant control for a class of nonlinear systems with sensor faults. International Journal of Control, Automation, and Systems. 2008;6(3):339–350.
7. Clarke F. Lyapunov functions and feedback in nonlinear control. in Optimal Control, Stabilization and Nonsmooth Analysis, in Lecture Notes in Control and Information Science, Springer, Berlin, Heidelberg, 2004:267–282. doi: 10.1007/978-3-540-39983-4_17.
8. Ando T. Schur complements and matrix inequalities: Operator-theoretic approach. in The Schur Complement and Its Applications, F. Zhang, Ed., in Numerical Methods and Algorithms, Boston, MA: Springer US, 2005:137–162. doi: 10.1007/0-387-24273-2_6.
9. Ahmed S, Amin AA, Wajid Z, Ahmad F. Reliable speed control of a permanent magnet DC motor using fault-tolerant H-bridge. Advances in Mechanical Engineering. Oct. 2020;12(10):168781402097031. doi: 10.1177/1687814020970311.
10. Shi S, Sun Y, Li X, Dan H, Su M. Moving integration filter-based open-switch fault-diagnosis method for three-phase induction motor drive systems. IEEE Transactions on Transportation Electrification. Sep. 2020;6(3):1093–1103. doi: 10.1109/TTE.2020.2999692.
11. Gholipour A, Ghanbari M, Alibeiki E, Jannati M. Speed sensorless fault-tolerant control of induction motor drives against current sensor fault. Electr Eng. Jun. 2021;103(3):1493–1513. doi: 10.1007/s00202-020-01179-0.
12. Dehbia O, Ahmed M, Ahmed C, Moussa B. Fault diagnosis techniques for electrical powertrain system- A review. in 2019 International Conference on Applied Automation and Industrial Diagnostics (ICAAID). Sep. 2019:1–7. doi: 10.1109/ICAAID.2019.8935003.
13. Li Y, Gong P. Fault-tolerant control of induction motor with current sensors based on dual-torque model. Energies. Jan. 2023;16(8):Art. no. 8. doi: 10.3390/en16083442.
14. Habibullah M, Debanath T, Sabbir MSH, Habibullah M, Debanath T, Sabbir MSH. Fault tolerant control of five-phase induction motor drive. IntechOpen, 2023. doi: 10.5772/intechopen.1001586.
15. Tousizadeh M, Che HS, Selvaraj J, Rahim NA, Ooi B-T. Fault-tolerant field-oriented control of three-phase induction motor based on unified feedforward method. IEEE Transactions on Power Electronics. Aug. 2019;34(8):7172–7183. doi: 10.1109/TPEL.2018.2884759.
16. Ahmad F, Alsuwian T, Amin AA, Adnan M, Qadir MB. Design of advanced fault-tolerant control system for three-phase matrix converter using artificial neural networks. IEEE Access. 2023:1–1. doi: 10.1109/ACCESS.2023.3320937.
17. Amin AA, Sajid Iqbal M, Hamza Shahbaz M. Development of intelligent fault-tolerant control systems with machine learning, deep learning, and transfer learning algorithms: A review. Expert Systems with Applications. Mar. 2024;238:121956. doi: 10.1016/j.eswa.2023.121956.
18. Alqarni ZA. Design of active fault-tolerant control system for multilevel inverters to achieve greater reliability with improved power quality. IEEE Access. 2022;10:77791–77801. doi: 10.1109/ACCESS.2022.3193790.
19. Yaacob S, Rasyadan A, Krishnanf P. Simulation analysis for induction motor drive fault detection and localization under variable load and speed operation. IOP Conf. Ser.: Mater. Sci. Eng. Mar. 2021;1127(1):012024. doi: 10.1088/1757-899X/1127/1/012024.
20. Adamczyk M, Orlowska-Kowalska T. Current sensors fault detection and tolerant control for induction motor drive. in 2021 IEEE 19th International Power Electronics and Motion Control Conference (PEMC). Apr. 2021:888–892. doi: 10.1109/PEMC48073.2021.9432575.
21. Gholipour A, Ghanbari M, Alibeiki E, Jannati M. Speed sensorless fault-tolerant control of induction motor drives against current sensor fault. Electr Eng. Jun. 2021;103(3):1493–1513. doi: 10.1007/s00202-020-01179-0.
22. Khlaief A, Saadaoui O, Abassi M, Chaari A, Boussak M. Open circuit fault detection and FTC for sensorless PMS motor control based on the back-EMF SMO. International Journal of Electronics. Feb. 2021;108(2):264–283. doi: 10.1080/00207217.2020.1793399.
23. Tabasian R, Ghanbari M, Esmaeli A, Jannati M. Control of three-phase induction machine drives during open-circuit fault: A review. IETE Journal of Research. Jul. 2022;68(4):2622–2639. doi: 10.1080/03772063.2020.1724833.
24. Saeed RB, Usman MH, Amin AA. Reliable speed control of a separately excited DC motor using advanced modified triple modular redundancy scheme in H-bridges. Advances in Mechanical Engineering. Jun. 2022;14(6):16878132221106289. doi: 10.1177/16878132221106289.
25. Gultekin MA, Bazzi A. Review of fault detection and diagnosis techniques for AC motor drives. Energies. Jan. 2023;16(15):Art. no. 15. doi: 10.3390/en16155602.
26. vall O. Mohamed M, Abdelaziz AY, Abo-Elyousr FK. Blockchain-based approach for load frequency control of smart grids under denial-of-service attacks. Computers and Electrical Engineering. May 2024;116:109150. doi: 10.1016/j.compeleceng.2024.109150.
27. Ajra Y, Hoblos G, Al Sheikh H, Moubayed N. A literature review of fault detection and diagnostic methods in three-phase voltage-source inverters. Machines. Sep. 2024;12(9):Art. no. 9. doi: 10.3390/machines12090631.
28. Tan L, Li Y, Liu C, Wang P, Li Z. Advanced voltage control methods for current source inverters with linear and nonlinear loads. in 2009 IEEE International Symposium on Industrial Electronics. Jul. 2009:1534–1539. doi: 10.1109/ISIE.2009.5217527.
29. Just H, Gentejohann M, Eggers M, Dieckerhoff S. Analysis and control of DC-link oscillations of voltage source inverters during unbalanced grid faults. in 2019 21st European Conference on Power Electronics and Applications (EPE '19 ECCE Europe). Sep. 2019:P.1–P.10. doi: 10.23919/EPE.2019.8914842.
30. Sensor Fault-Tolerant Control of Induction Motor Drives: An Important Topic to Research | LinkedIn. Accessed: Apr. 04, 2024. [Online]. Available: https://www.linkedin.com/pulse/sensor-fault-tolerant-control-induction-motor-drives-topic-das-ph-d/